LES-based Numerical Analysis of Surface-Pressure Fluctuations and Unsteady Thrust of a Marine Propeller

Jin Tian[1]; Haosen Yang[2]; Zhenguo Zhang[3]; Guoqing Yuan[4];
Zhiqiang Rao[5]; Hongxing Hua[6];
Institute of vibration, shock and noise, Shanghai Jiao Tong University, China

ABSTRACT

Fluctuating forces induced by a rotating marine propeller are major sources exciting the hull vibration which radiates unwanted underwater noise. To attain a better understanding of the fundamental nature of these excitation sources, a numerical study of blade surface-pressure fluctuations and unsteady thrusts of a marine propeller is performed. A computational model based on large eddy simulation (LES) with moving mesh technique is developed. Considering both of the uniform and non-uniform inflow conditions, the hydrodynamics performances including (i) the spatial variation of the vortex structure; (ii) fluctuating forces acting on the propeller blades; and (iii) the unsteady propeller thrust are obtained in time and frequency domains with reasonable accuracy. The correlation of the vortex structures to pressure fluctuations is evaluated through visualizing the pressure distribution on the blades. The spectral characteristics of the blade surface-pressure and the unsteady thrust are then analyzed and compared for the two different inflow conditions. Numerical results show that clear peak frequencies of the surface-pressure spectrum are related to the harmonics of shaft frequency, and inflow uniformness significantly affects the unsteady thrust spectrum.

Keywords: Surface-Pressure Fluctuations, Underwater noise, Unsteady Thrust

1. INTRODUCTION

With the rotation of the propeller, fluctuating forces which is generally unsteady may lead to vibrations and sound radiations of the propeller. When forces are hydrodynamic in origin, the sounds radiated directly into the fluid are independent of any motion on a fluid boundary (1). Physically, the flow field of a propeller is inherently unsteady attributed to the vortex-blade interaction, the viscous flows, vortex shedding and so on. Although this phenomenon is extremely familiar, little investigation on propeller blade surface-pressure fluctuations has been experimentally or theoretically carried out during the past decades. Hence, the real situation of fluctuating pressure on blade surface is still poorly understood.

Several practical methods have been reasonably proposed in the literature to study the unsteady hydrodynamics of propeller operating in uniform or nonuniform wake, including the experimental method (6), theoretical method (5) and numerical method (7-10), such as unsteady Reynolds Average Navier Stokes (URANS) and large eddy simulation (LES). Concerning the rotating blades of turbomachinery, Wang et al. measured the unsteady pressure fluctuations on the blade suction surface of an axial compressor with five high response miniature pressure transducers mounting along a streamline at 50% span of the rotor blades (2). Jang et al. (3, 4) observed experimentally the three-dimensional structure of the vortical flow field in a propeller fan with a shroud covering only the rear region of its rotor tip using LDV measurements. Numerical analyses were also conducted with a large eddy simulation (LES) (3, 4).

In the present work, a numerical study of blade surface-pressure fluctuations and unsteady thrusts

[1] tianjinsjtu@sjtu.edu.cn
[2] yanghaosen@sjtu.edu.cn
[3] zzgjtx@sjtu.edu.cn
[4] yuan_weizhao@163.com
[5] raozhiqiang@sjtu.edu.cn
[6] hhx@sjtu.edu.cn

of a marine propeller is performed. The propeller excitations are computed by using LES and moving mesh technology. A CFD computation software, FLUENT, is used to simulate the hydrodynamics fields of the propeller, and LMS Virtual.Lab software is utilized to perform post-processing of the obtained CFD results.

2. LARGE EDDY SIMULATION

The turbulent flow can be described by Navier-Stokes equations without any turbulence modeling. With direct numerical simulation (DNS), Navier-Stokes equations can be solved directly. However, DNS is quite computation consuming since all the lengthscales and timescales should be resolved. It is estimated that the number of mesh cells required for incompressible free turbulence is about $Re^{9/4}$. The application of DNS is limited to flows at moderate Re due to prohibitive computational cost. Considering the computational cost, LES is selected for the hydrodynamic field simulation.

2.1 Large Eddy Simulation

LES is capable of solving three-dimensional and transient turbulent flow problems. The large scales can be solved directly, whereas the small scales are modeled with SGS model. In FLUENT, the finite-volume discretization provides the filter operation:

$$\bar{\Phi}(x) = \frac{1}{V}\int_{v} \bar{\Phi}(x')dx', \quad x' \in v \tag{1}$$

where V is the volume of a computational cell. The governing equation for LES is derived by filtering the time-dependent incompressible Navier-Stokes equations as,

$$\frac{\partial \bar{u}_i}{\partial t} + \frac{\partial}{\partial x_j}(\bar{u}_j \bar{u}_i) = -\frac{\partial \bar{p}}{\partial x_i} + \nu \frac{\partial}{\partial x_j}\left(\frac{\partial \bar{u}_i}{\partial x_j} + \frac{\partial \bar{u}_j}{\partial x_i}\right) - \frac{\partial \tau_{ij}}{\partial x_j}, \frac{\partial \bar{u}_i}{\partial x_i} = 0, \tag{2}$$

where τ_{ij} is the SGS stress tensor defined by

$$\tau_{ij} = \overline{u_i u_j} - \bar{u}_i \bar{u}_j \tag{3}$$

A SGS model is required to model the SGS eddy viscosity. For the Smagorinsky-Lilly model,

$$\mu_t = \rho L_s^2 \sqrt{2\bar{S}_{ij}\bar{S}_{ij}} \tag{4}$$

$$L_s = \min(kd, C_s(\Delta x \Delta y \Delta z)^{1/3}) \tag{5}$$

where L_s is the mixing length for the subgrid scales; d is the distance to the closest wall; k is the von Karman constant; and C_s is the Smagorinsky constant. It has been found that C_s=0.1 yields the best results for a wide range of flows.

3. NUMERICAL MODELING

The governing equations are discretized with the finite-volume method, which is employed to perform LES simulations. Both the geometric model creation and the mesh generation are carried out by HyperMesh software. Moreover, the post-processing procedure is accomplished using CFD-Post and LMS Virtual.Lab.

3.1 Moving Mesh Technique

The moving mesh model allows one to set up a problem in which separate zones move relative to each other. The motion can be either translational or rotational. The relative motion of stationary and moving components will give rise to transient interactions. The transient solution sought in a moving mesh simulation is generally time-periodic. That is, the transient solution repeats with a period related to the speeds of the moving domains.

In the moving mesh technique, two or more cell zones are used. Each cell zones are associated with one another to form a “mesh interface.” The two cell zones will move relative to each other

along the mesh interface. During the calculation, the cell zone move relative to one another along the mesh interface in discrete steps.

3.2 Computational domain and boundary conditions

A circular cylinder is chosen as the computational domain, which has a diameter of 4*D* (*D*=250mm, the diameter of the considered propeller) and a dimension of 10*D* in the streamwise direction (-3<*x/D*<7). The rotating zone is a concentric cylinder, which has a diameter of 1.2*D* and a dimension of 0.8*D* in the streamwise direction (-0.4<*x/D*<0.4). The nonuniform inflow is produced by a "+" type bluff body, as shown in Figure 1. The main dimensions of the propeller model are given in Table 1. The whole computational domain is meshed with unstructured tetrahedral cells and structured hexahedral cells. Figure 2 demonstrates the mixed cells around the rotating zone and a single blade.

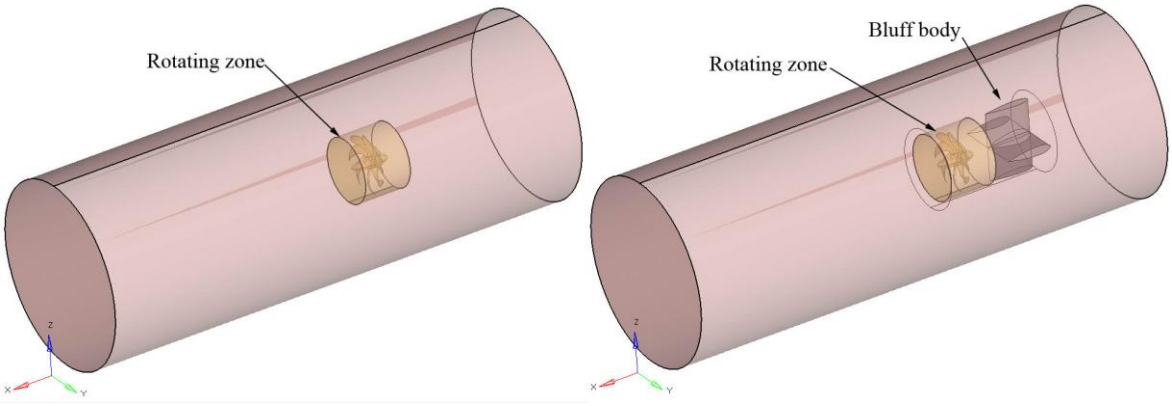

Figure 1 – The model of solution field for uniform inflow (left) and nonuniform inflow (right)

Table 1 – Propeller parameters

Model propeller parameters	
Diameter	*D*=250mm
Number of blades	7
Pitch ratio	1.1
Hub ratio	0.2

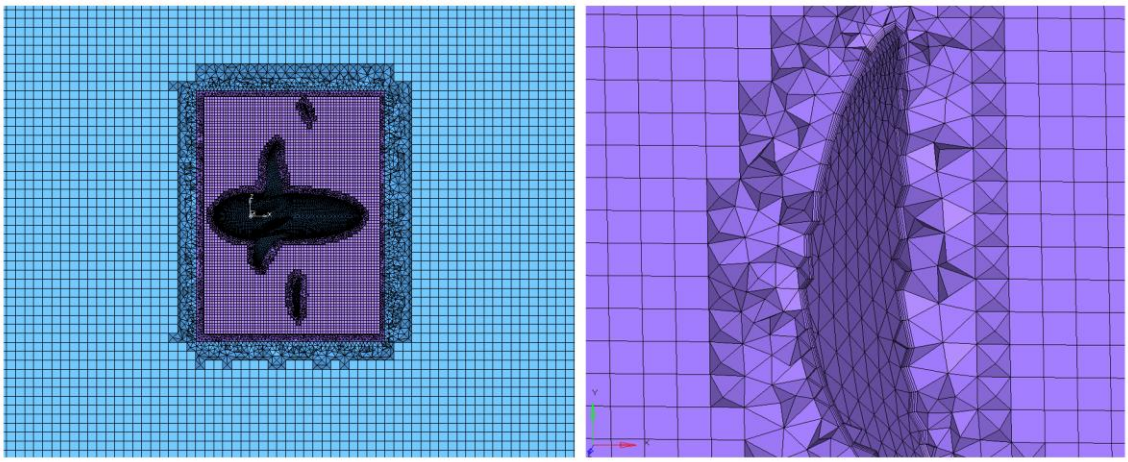

Figure 2 – The mesh around the rotating zone (left) and single blade (right)

The number of grids for uniform inflow calculation is about 5.7 million, and for nonuniform inflow calculation is about 6.8 million. The velocity inlet boundary condition is set for the flow inlet and the cylindrical surface. A pressure outlet is set for the flow outlet. No-slip boundary condition is applied to the propeller wall.

In the case of uniform inflow, the rotational speed of the propeller is 600 rpm, and the inlet velocity is 1.25 m/s with an advance coefficient *J*=0.5.

In the case of nonuniform inflow, the rotational speed of the propeller is 1200 rpm, and the inlet velocity is 3.5 m/s with an advance coefficient J=0.7.

3.3 Discretization Scheme

The pressure-based solver is used for the simulations. Time step Δt=8E-5s is selected for the calculation to ensure that convergence can be obtained in each time step. SMPLE scheme is used for the pressure-velocity coupling. Bounded central differencing scheme is employed for the momentum equation and the second-order implicit is used for the transient formulation.

4. RESULTS AND DISCUSSION

The computational results are obtained including 1) the vortex structure of the propeller operating in uniform inflow, 2) propeller blade surface-pressure fluctuations operating in uniform inflow, and 3) propeller blade surface-pressure fluctuations operating in nonuniform inflow, which are given respectively in following sub-sections.

4.1 Vortex structure

The result of an instantaneous LES solution is analyzed, and Q-criterion is used to identify the vortex. Instantaneous vorticity and static pressure distribution at 96% blade height are shown in Figure 3. It can be seen that a high strength tip vortex region downstream of the blade tip. Moreover, the shedding tip vortex can be observed from the low-pressure core distribution. Figure 4 illustrates the complex flow environment near the blade tip. The corresponding vortex structure can be found in Figure 5, which is displayed as isosurfaces of Q=8000. Trailing edge vortex and tip vortex can also be seen in Figure 5.

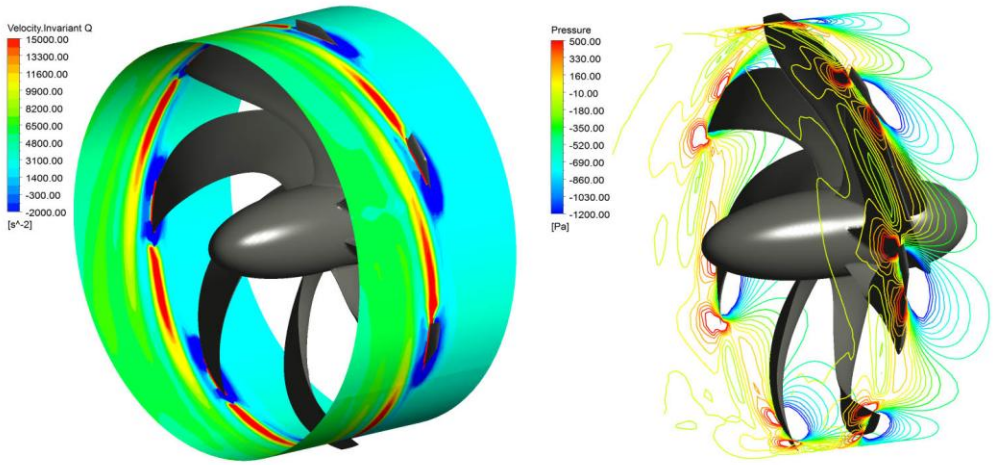

Figure 3 – Vorticity (left) and static pressure (right) distribution at 96% blade height

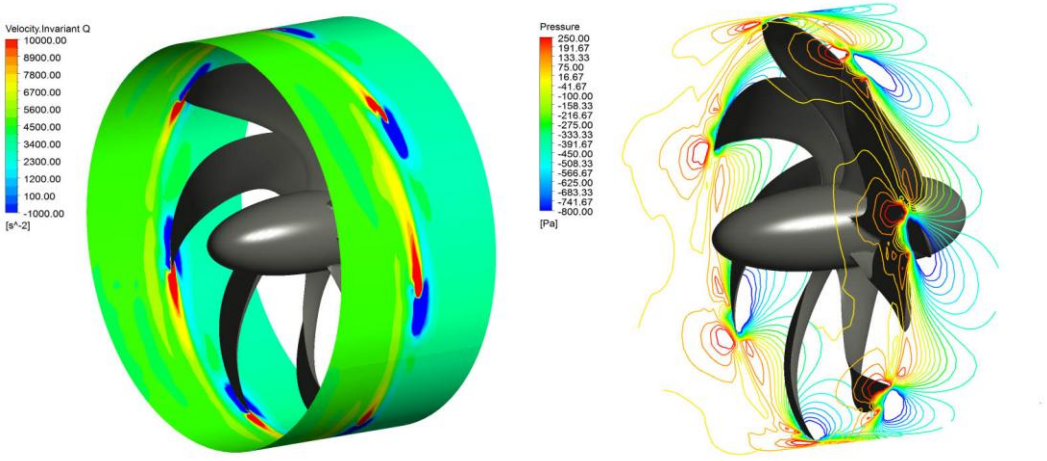

Figure 4 –Vorticity (left) and static pressure (right) distribution at 100% blade height

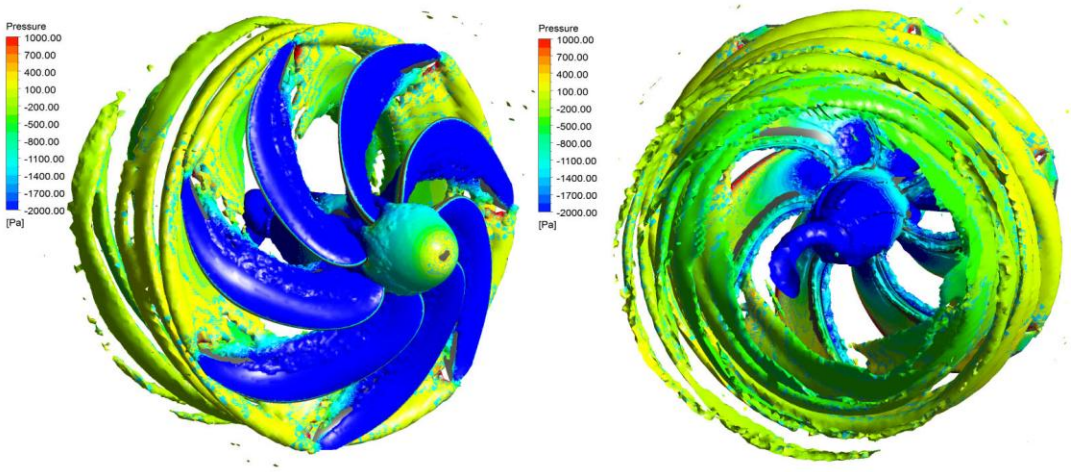

Figure 5 – *Q* isosurfaces, *Q*=8000, colored by static pressure

4.2 Blade Surface-Pressure

By monitoring the fluctuating static pressure on trailing edge as shown in Figure 6, the spectrum properties are obtained. The sampling interval is set as 8E-5s, and the frequency resolution is 1Hz. The frequency spectrum with regard to the trailing edge is obtained from 22 points.

In the case of uniform inflow, the axial passing frequency (APF) is 10Hz. Figure 7 illustrates the pressure frequency spectrum of A and B. The fluctuating pressure is tonal at shaft harmonics, and the maximum peaks in amplitude appear at 4APF, 8APF, and 12APF, respectively. These spectrum properties are mainly contributed to the vortex shedding from the blade. The vorticity distribution and peak values of 22 points along trailing edge at 4APF are given in Figure 8.

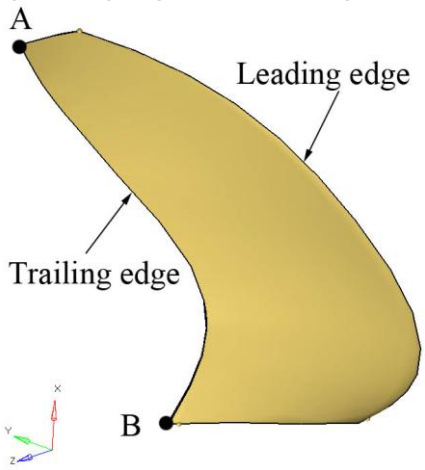

Figure 6 – Location of the pressure monitors on trailing edge

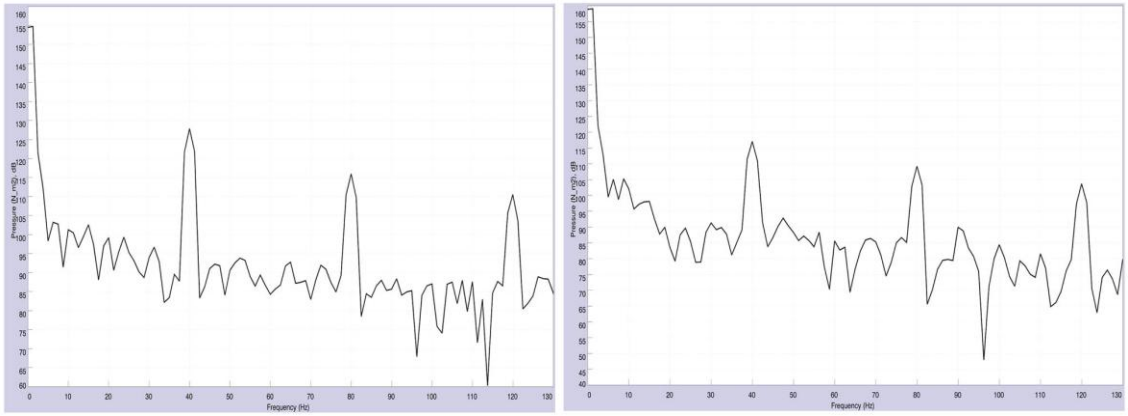

Figure 7 – Frequency spectrum of A (left) and B (right) in uniform inflow

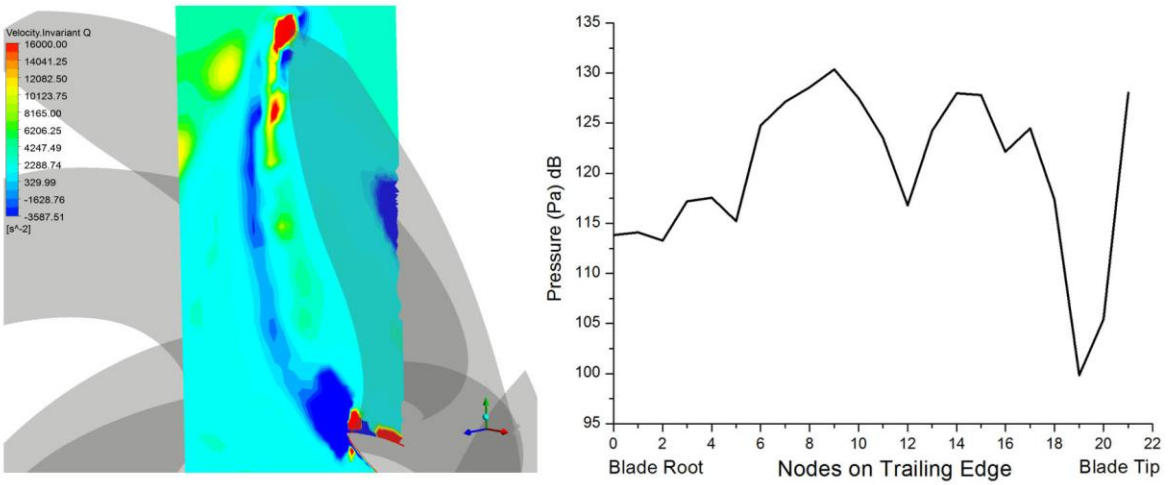

Figure 8 – Vorticity distribution (left) and pressure peak values (right) at 4APF along trailing edge

From the cross-sectional cut in Figure 8, it can be found that the variation in vorticity strength is close to the variation in pressure peak values.

In the case of nonuniform inflow, the axial passing frequency (APF) is 20Hz. The pressure frequency spectrum of A and B is illustrated in Figure 9.The fluctuating pressure is tonal at shaft harmonics, but none special characteristics can be found from the peak values as compared to that in uniform inflow.

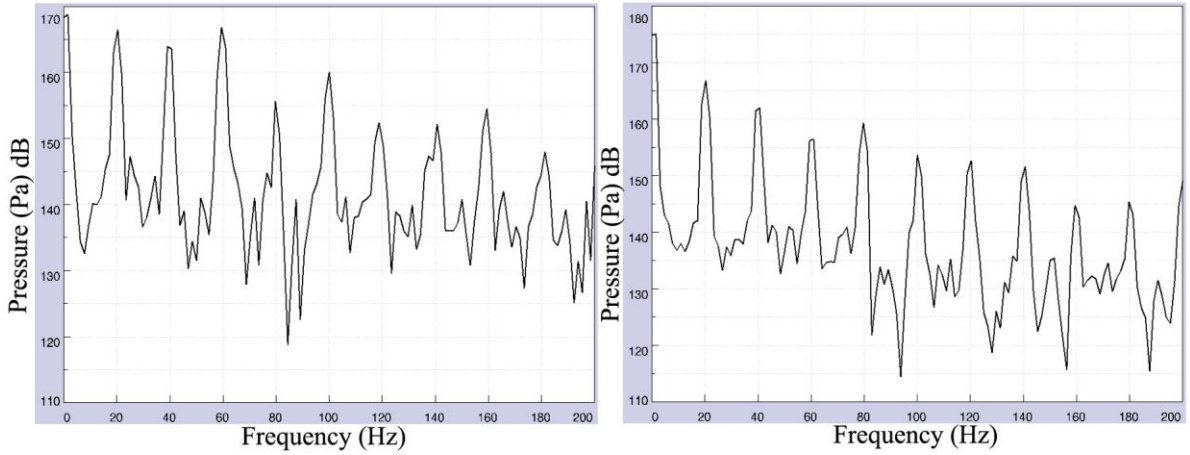

Figure 9 – Frequency spectrum of A (left) and B (right) in nonuniform inflow

From above simulation results, it can be concluded that:

(1) In the case of uniform inflow, the fluctuating pressure is tonal at shaft harmonics, and the maximum peaks in amplitude appear at 4APF, 8APF, 12APF.

(2) The variation in vorticity strength is highly correlated to that in pressure peak values, along trailing edge.

(3) In the case of nonuniform inflow, the fluctuating pressure is tonal at shaft harmonics, but none special characteristics can be observed.

4.3 Blade Unsteady Thrust

In this sub-section, the unsteady thrust T_b of a single propeller blade in nonuniform inflow is studied. This unsteady thrust is caused by the variation in the inflow to the propeller. The quantity T_b is an important parameter in analyzing the ship noise, since it may cause a propeller to vibrate which radiates underwater noise.

Figure 10 shows the axial velocity distribution induced by the "+" type bluff body. When the blade encounters these four low velocity regions, the blade becomes heavy loading.

Figure 11 shows the time history of the thrust T_b during two cycles and frequency spectrum of T_b. The unsteady blade thrust T_b is tonal at 1APF and 4APF, this is due to the interaction between the blade and nonuniform wake of the "+" type bluff body. The peak at 1APF is due to the asymmetric distribution of axial velocity. The steady component of T_b is 32.03N, and unsteady component at

4APF is 2.27N, on the order of 7% of the steady thrust.

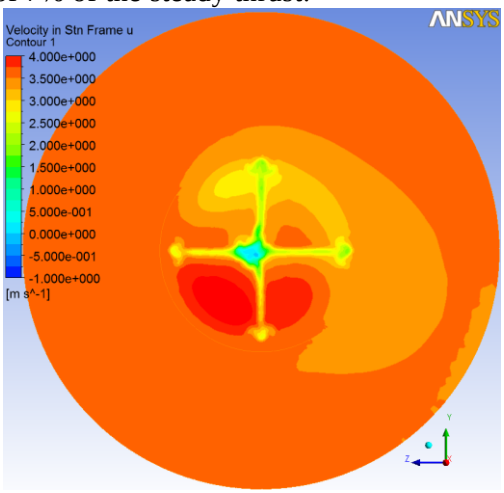

Figure 10 – Contour of axial velocity on yz plane at *x/D*=-0.45

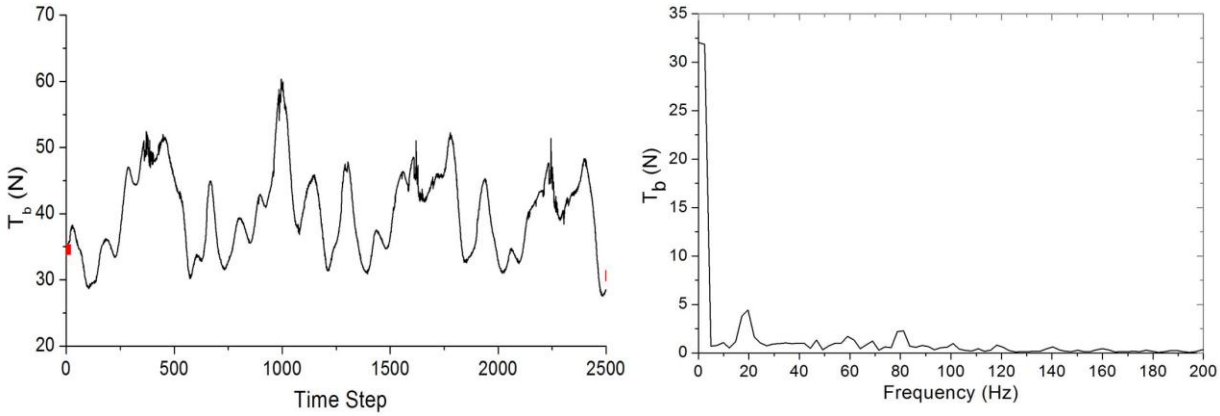

Figure 11 – Time history of blade thrust T_b (left) and frequency spectrum of T_b (right)

5. CONCLUSIONS

A numerical study of blade surface-pressure fluctuations and unsteady thrusts of a model propeller is presented. The CFD computations are performed using large eddy simulation together with the moving mesh technique. The complex swirling flow of the propeller is investigated. The vortex structure is evaluated through visualizing the vorticity and pressure distribution. The tip vortex and trailing edge vortex can be clearly found from the *Q* isosurfaces. It is found that the variation in vorticity strength is close to the variation in pressure peak values along trailing edge.

The fluctuating blade surface-pressures in both the uniform and nonuniform inflow are calculated, which are observed to be tonal at shaft harmonics for both cases. Also, the maximum peaks in amplitude are found to appear at 4APF, 8APF and 12APF, respectively. Furthermore, little difference in special characteristics can be seen from the peak values in nonuniform inflow as compared to that in uniform inflow. The characteristic generalized from the numerical results agrees well with those experimental results for an axial compressor rotor blade in Ref.2.

The unsteady blade thrust T_b operating behind a "+" type bluff body is found to be tonal at 4APF, which is largely due to the interaction between the blade and four low velocity regions. As is observed clearly, the unsteady component at 4APF accounts for about 7 percent of the total steady thrust. Moreover, in the present work the peak at 1APF is mainly attributed to the asymmetric of the four low velocity regions, which is different from the computational results presented in Ref.8, Further work should be done to clarify what causes this difference.

REFERENCES

1. D. Ross. Mechanics of Underwater Noise. Los Altos, California, USA: Peninsula Publishing; 1987.
2. Wang Q. Experimental Investigation of Unsteady Pressure on an Axial Compressor Rotor Blade Surface. Energy and Power Engineering. 2010;02(02):131-6.
3. Jang C-M, Furukawa M, Inoue M. Analysis of Vortical Flow Field in a Propeller Fan by LDV Measurements and LES—Part I: Three-Dimensional Vortical Flow Structures. Journal of Fluids Engineering. 2001;123(4):748
4. Jang C-M, Furukawa M, Inoue M. Analysis of Vortical Flow Field in a Propeller Fan by LDV Measurements and LES—Part II: Unsteady Nature of Vortical Flow Structures Due to Tip Vortex Breakdown. Journal of Fluids Engineering. 2001;123(4):755.
5. R. J. Boswell, M. L. Miller. Unsteady Propeller Loading Measurement, Correlation with Theory, and Parametric Study. Technical Report. Department of the Navy Naval Ship Research and Development Center; 1968.
6. S. Jessup. Measurement of Multiple Blade Rate Unsteady Propeller Forces. Technical Report. 1990: DTRC-90/015.
7. V. Krasilnikov, Z. Zhang, F. Hong. Analysis of unsteady propeller blade forces by RANS. Proc First International Symposium on Marine Propulsors; June 2009; Trondheim, Norway.
8. M. Lesfvendahl, C. Troeng. Computation of cycle-to-cycle variation in blade load for a submarine propeller using LES. Proc Second International Symposium on Marine Propulsors; June 2011; Hamburg, Germany.
9. Shamsi R, Ghassemi H, Molyneux D, Liu P. Numerical hydrodynamic evaluation of propeller (with hub taper) and podded drive in azimuthing conditions. Ocean Engineering. 2014;76:121-35.
10. Wei Y, Wang Y. Unsteady hydrodynamics of blade forces and acoustic responses of a model scaled submarine excited by propeller's thrust and side-forces. Journal of Sound and Vibration. 2013;332(8):2038-56